COBEM 2023 27TH INTERNATIONAL CONGRESS OF MECHANICAL ENGENEERING

ABCM Brazilian Society of Mechanical Sciences and Engineering
27th ABCM International Congress of Mechanical Engineering
December 04-08, 2023, Florianópolis-SC, Brazil

COB-2023-1394
EXPERIMENTAL IDENTIFICATION OF DRAG HYDRODYNAMIC PARAMETERS FOR AN OPEN FRAME ROV USED IN THE STOCK ASSESSMENT OF SCALLOPS

Paola Andrea Fonseca Florez
Universidade Federal do ABC
paola.fonseca@ufabc.edu.br

Richard Anthony Huamani Reátegui
Veox
rhuamani@veox.tech

Juan Pablo Julca Avila
Universidade Federal do ABC
juan.avila@ufabc.edu.br

Abstract. *This work presents the experimental method to identify the hydrodynamic drag parameters in each degree of freedom of an open frame underwater vehicle to the stock assessment of Peruvian scallops. It describes the mechanical project and hardware used to make the experiments. The method, known as self-propelled tests, is applied to each degree of freedom individually. Then, the drag coefficient and the operating range of the Reynolds number were calculated with the data collected from the tests. The drag coefficient calculated to the linear motions was almost constant in the Reynolds number range between* 0.4×10^5 *to* 1.8×10^5*, and the drag coefficient calculated to the angular motion was almost constant in the Reynolds number range between* 1.5×10^5 *to* 6×10^5*. The linear and quadratic drag parameters were determined by the least square method in each degree of freedom of the vehicle. The drag parameter values found by the experiments have coherence because the higher parameter value corresponds to the larger projected area, and the lower parameter value to the smaller projected area. The main perturbation force of the vehicle when it moves in the heave direction is the buoyancy force, which coincides by 3% with the perturbation value obtained by the method of least squares, demonstrating that the procedure followed to determine the hydrodynamic parameters is correct.*

Keywords: *Open-frame underwater vehicle, experimental identification of parameters, hydrodynamic modelling, least square method*

1. INTRODUCTION

The stock assessment of scallops is a critical task in the production process of these benthic animals in the sea. Divers do this activity, but it puts their health in danger, is expensive, and demands much time. A possible solution is using a ROV (Remotely Operated Vehicle). The vehicle designed for this work is called Hindrax, and it will help the fishermen do the stock assessment of scallops safer and in less time. The Hindrax ROV has a vision system implemented into the recordings taken by its camera located at the bottom, letting it know the quantity and size of the scallops. The motion control of this vehicle depends mainly on the ability of the operator and the maritime conditions (ocean currents or wind) that can become a tedious task because the recordings taken by the Hindrax ROV must be stable for processing by the detection algorithm of the scallops. Therefore, the control system of the Hindrax ROV should be designed based on a mathematical model. The mathematical model includes the hydrodynamic parameters that need to be determined. Those parameters will help design the control system for the Hindrax ROV.

The hydrodynamic parameters of an underwater vehicle are classified into two types: The drag parameters due to the fluid viscosity, and the added mass parameters due to the fluid inertia. Numerical and experimental methodologies can identify those parameters. The numerical method uses CFD (Computational Fluid Dynamics) software. Such as, Randeni. *et al.* (2015) developed a CFD model to replicate the pure sway motion of a vehicle that is operated close to a larger moving vehicle. The experimental methods to identify the hydrodynamic parameters use external equipment or the self-propulsion system of the vehicle. Some examples of the use of external equipment are: Ross *et al.* (2015) used a PMM (Planar Motion Mechanism) to determine the hydrodynamic coefficients. The towing carriage of the PMM moved the vehicle at different constant velocities through a water channel while the drag force was measured by a load cell. Zhandong *et al.* (2017) used another kind of PMM; they fixed a vehicle in a circulating water channel and attached it to a six-axis force sensor; the water flowed to different velocities while the drag force was measured. Eng *et al.* (2008)

proposed an experimental method based on the pendulum swing motion to identify the hydrodynamic parameters in the surge, sway and heave directions, and a torsion pendulum for the yaw motion. The present work focuses on self-propelled tests and using on-board sensors to determine the hydrodynamic drag parameters of the Hindrax ROV.

In 1990, Goheen and Jefferys (1990) proposed one of the first experiments to determine the hydrodynamic parameters for ROV called "UMEL SeaUp" that did not require a towing tank or a PMM. Instead, the vehicle made some maneuvers in a tank of water while a navigation system measured the velocity, position, heading, and force generated by its thrusters. They did an experiment that stimulated every thruster and degree of freedom and, with the data collected, estimated the hydrodynamic parameters using the identification system ARMAX (Auto-regressive moving average model with exogenous inputs).

Self-propelled tests also allow us to determine the hydrodynamic parameters in rotation motions. Such as, in Miskovic *et al.* (2011), the hydrodynamic parameters were determined by inducing the system into self-oscillation in the yaw motion. The vehicle was rotated clockwise and counterclockwise by applying known moments to a commercial ROV called Videoray while the angular velocity was measured. They proposed a novel method called IS-O to determine the hydrodynamic parameters that gave similar results to those obtained using a least square method.

The identification procedure of the hydrodynamic parameters proposed by Avila *et al.* (2013) was based on the self-propelled tests at constant and variable velocities using an ROV called LAURS. First, the coefficients of the thruster's model were experimentally determined by putting each thruster at bollard-pull conditions. Then, the efficiency coefficients of the system of thrusters operating close to the vehicle structure were defined in order to know the real force at which the vehicle moved in the self-propelled tests. Finally, the self-propelled tests were made in a pool while the DVL (Doppler Velocity Log) measured the velocity. The LS (Least Square method) determined the hydrodynamic parameters from the data collected in the tests. The values of the parameters obtained from self-propelled tests were consistent with those obtained using a PMM.

This work presents the results and the procedure to determine the hydrodynamic drag parameters of the open-frame ROV called Hindrax in 6-DOF (Degree of Freedom). First, the force generated by each thruster was determined under bollard pull conditions to calculate the torque/force applied upon the vehicle during its motion. Next, the vehicle moved at different constant velocities in 1-DOF, and the on-board sensors as DVL and gyroscope allowed us to find the linear and angular velocities, respectively. Finally, the parameter identification method of LS was used to determine the linear and quadratic drag parameter values using the data collected in the self-propelled tests. This work also describes the mechanical project and the hardware used in the experiments.

2. Hindrax ROV design

2.1 Mechanical design and sensory system

The Hindrax ROV is an observation class mini ROV capable of submerging up to 60 m below. The vehicle's main frame is made of acrylic, and the structural joints, the supports for pressure vessel and thrusters were made of PETG polyethylene terephthalate glycol) using a 3D printer (see Figure 1). The upper part of the vehicle has two thin-walled tubes that work as floats, and there is a pressure vessel made of acrylic for the on-board electronics. The bottom of the vehicle consists of a pressure vessel for the battery and two PETG tubes containing the ballasts. The pressure vessels have o-rings in their flanges and caps to ensure hermeticity.

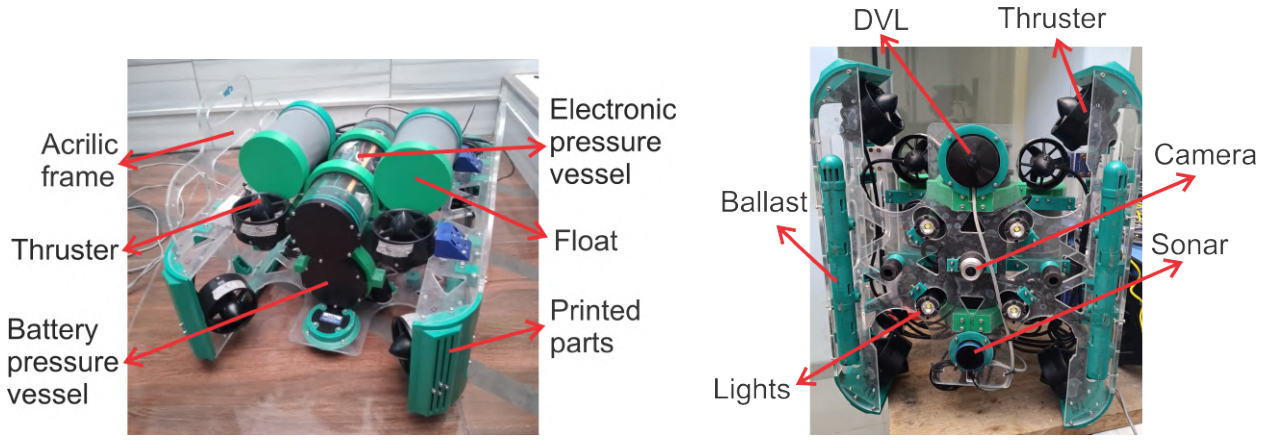

(a) (b)

Figure 1: ROV Hindrax: (a) upper view; (b) bottom view

The Hindrax ROV has two symmetry planes conformed by the xz and yz axes, as it is shown in Figure 2. The vehicle

size is 0.59 m, 0.47 m, and 0.4 m in length, width, and height, respectively. It has positive buoyancy with a force of 0.83 N, which means the vehicle floats when its thrusters are turned off. The total mass of the Hindrax ROV is 15.22 kg, and its volume is 0.0153 m^3.

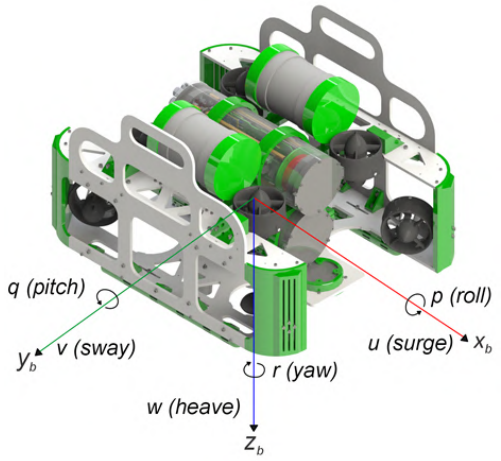

Figure 2: Frame of reference of the Hindrax ROV.

The Hindrax ROV is powered by an on-board battery of 14.8V, 19.2Ah that gives the vehicle an autonomous operation time of 2.5 hours in normal use mode and 5 hours in light use mode. The on-board electronics comprise sensors and actuators that are controlled by the microcontroller STM32F407VGT6 and the single-board computer Raspberry PI 4. The ESCs (Electronic Speed Control) are connected to the thrusters to control their velocities. The microcontroller sends PWM (pulse width modulation) signals to the ESC to change the thruster velocity. PWM signals also control the light intensity.

Table 1: Hindrax sensors description

Variable	**Sensor**	**Communication**	**Precision**
Velocity (surge and sway)	DVL-75(Cerulean)	Serial	Mean error: 5% of distance traveled
Angular position	IMU inside of DVL-75(Cerulean)	Serial	Depends on its calibration
Accelerations (x ,y and z)	Accelerometer(ICM-20948)	I2C	Full scale range of ±2 , ±4 g, ± 8g, and ±16 g
Angular velocities	Gyroscope(ICM-20948)	I2C	Full-scale range of ±250 dps, ±500 dps, ±1000 dps, and ±2000 dps
Heading	Magnetometer(ICM-20948)	I2C	Wide range to ±4900 µT
Depth	Pressure(MS5837)	I2C	± 0.007 PSI
Altitude	Sonar(BlueRobotics)	Serial	Resolution of 0.5%

The sensory system is described in Table 1. The system is composed of the following elements. There is a sonar that measures the altitude. There is also the inertial unit IMU ICM-20948 that contains an accelerometer, gyroscope, and magnetometer to know the acceleration, angular velocity, and heading, respectively. It incorporates a Doppler effect sensor DVL-75 that measures the velocity in the surge and sway direction. This sensor also has inside a magnetometer that measures the angular position. Finally, there is a pressure sensor based on the sealed pressure unit MS5837 that measures the depth. Figure 3 illustrates the on-board electronics and sensors distribution of the electronics pressure vessel.

The communication between the Hindrax ROV and the remote operation station is through a tether cable of neutral buoyancy using an Ethernet protocol and two communication boards, one inside the electronics pressure vessel connected to the Raspberry PI 4 and the tether cable, and the other on the remote operator station. The remote operator station has a PC and a communication board, which is a USB to Ethernet adapter connected to the PC and to the tether cable. In that way, the operator can control the vehicle sending commands from a terminal window in the PC to the Raspberry PI 4, and extract the sensors' measurements previously stored on the Raspberry's memory.

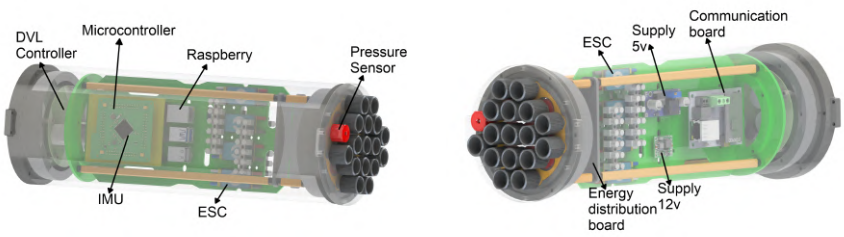

(a) (b)

Figure 3: Electronics pressure vessel (a) right view; (b) left view

2.2 Propulsion system

The Hindrax ROV has eight thrusters that let it move in 6-DOF. They are divided into two layers: four thrusters at the top layout provide power for the heave, roll, and pitch motion, and the remaining thrusters at the bottom layout allow the motion in the surge, sway, and yaw motion as Figure 2 illustrates.

2.2.1 Thruster parameter identification

Experimental tests under bollard-pull conditions determined the thrust curves of the thrusters. Figure 4a illustrates the experimental setup. A load cell at the top of the support tube measured the force generated by the thruster. Then, Archimedes' law of the lever was used to calculate the thrust at different PWM signals. The ESC of the thruster allows control of the thruster's velocity and the rotational direction. These controllers received PWM values in a range of 1100 to 1900 µs. The value of 1500 µs was for stopping the motor, 1100 – 1500 µs for the negative rotation, and 1500–1900 µs for the positive rotation.

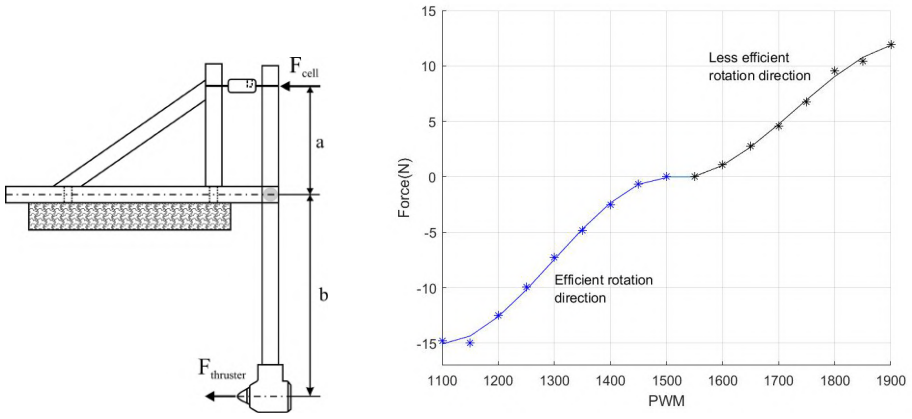

(a) (b)

Figure 4: (a) Experimental setup for the identification of the thruster's curve.(b) Thrust curve for one of the thrusters.

The thrust curve of one of the thrusters is illustrated in Figure 4b. The following cubic polynomial is considered to model the thrust,

$$\tau = c_4 P^3 + c_3 P^2 + c_2 P + c_1, \tag{1}$$

Where P is the PWM signal sent by the microcontroller to the thruster, and c_1, c_2, c_3, and c_4 are the coefficients identified by the LS method. Table 2 shows the values of the coefficients that correspond to the thrust curve of the thruster in Figure 4b with negative and positive rotation.

All thrusters were tested, and the coefficient values from one thruster with the others were similar.

Table 2: Parameter of the thrust model from one of the thrusters

	c_4	c_3	c_2	c_1
Negative direction	-4.61×10^{-7}	0.001794	-2.2726 ± 0.3212	927.1827 ± 137.82
Positive direction	-3.52×10^{-7}	1.82×10^{-4}	-0.3106 ± 0.0826	174.3542 ± 47.28

3. Dynamic model and identification technique of parameters

The motion of the Hindrax ROV with constant velocity ξ in still water and the hydrodynamic force F_ξ that opposes its motion is given by,

$$F_\xi = k_{\xi|\xi|}\xi\,|\xi| + k_\xi\xi + b_\xi, \tag{2}$$

where the first and second terms on the right side are the quadratic and linear drag forces, respectively, $k_{\xi|\xi|}$ being the quadratic coefficient, k_ξ the linear coefficient, and the third term b_ξ is the force that represents the modeling errors or the noise measured by the sensors. In Eq. 2, ξ is experimentally measured, and the absolute value symbol is to conserve the velocity sign. When ξ is subscripted, it indicates the DOF of the vehicle's motion. The vehicle was tested in their 6-DOF. Accordance to the marine vessel notation ξ is equal to u, v, and w in the surge, sway, and heave motions, respectively, or p, q, and r in roll, pitch, and yaw rotations, respectively (see Figure 2).

The parameter identification method we used in this work to find the hydrodynamic drag parameters was the least square method (LS). This method finds the best-fitting curve for a set of experimental data points. It was used in Goheen and Jefferys (1990), and Avila *et al.* (2013). They demonstrated that the LS efficiently identifies the added mass parameters, and the linear and quadratic drag coefficients of underwater vehicles from the data collected by self-propulsion tests.

Eq. 2 is written as an experimental data set using a second-order polynomial regression as,

$$\underbrace{\begin{Bmatrix} f_1 \\ f_2 \\ f_3 \\ \vdots \\ f_n \end{Bmatrix}}_{\mathbf{Y}} = \underbrace{\begin{bmatrix} x_1^2 & x_1 & 1 \\ x_2^2 & x_2 & 1 \\ x_3^2 & x_3 & 1 \\ \vdots & \vdots & \vdots \\ x_n^2 & x_n & 1 \end{bmatrix}}_{\mathbf{X}} \underbrace{\begin{bmatrix} k_{\xi|\xi|} \\ k_\xi \\ b_\xi \end{bmatrix}}_{\boldsymbol{\theta}} + \underbrace{\begin{bmatrix} \mathcal{E}_1 \\ \mathcal{E}_2 \\ \mathcal{E}_3 \\ \vdots \\ \mathcal{E}_n \end{bmatrix}}_{\boldsymbol{\mathcal{E}}}, \tag{3}$$

Where n is the total number of observed points, f_n represents the forces measured in the discrete points, x_n^2 and x_n, the velocity squared and velocity itself, which go with the discrete point of force and $\mathcal{E}_n$, the residual values,respectively. The last equation is written in vectorial form as,

$$\mathbf{Y} = \mathbf{X}\boldsymbol{\theta} + \boldsymbol{\mathcal{E}}, \tag{4}$$

where $\mathbf{Y}$ is the output vector of size n that contains the forces measured and $\mathbf{X}$ is the regression matrix of size $n \times 3$, which contains the velocity prediction observations. $\boldsymbol{\theta}$ is the parameters vector of the system, and $\boldsymbol{\mathcal{E}}$, the vector of the prediction errors.

The total sum of the squares S of the residuals between the discrete points and the mean predicted is given by,

$$S = (\mathbf{Y} - \mathbf{X}\boldsymbol{\theta})^T(\mathbf{Y} - \mathbf{X}\boldsymbol{\theta}). \tag{5}$$

The LS method seeks to determine the vector $\boldsymbol{\theta}$ which minimizes S. Differentiating Eq. 5 with respect to $\boldsymbol{\theta}$ and setting the result to zero, is obtained the LS estimator $\hat{\boldsymbol{\theta}}_{\mathbf{LS}}$, see Payne and Goodwin (1977),

$$\hat{\boldsymbol{\theta}}_{LS} = [\mathbf{X}^T\mathbf{X}]^{-1}\mathbf{X}^T\mathbf{Y}, \tag{6}$$

If we assume that the components of the vector $\boldsymbol{\mathcal{E}}$ are of zero mean, are independent and have known variances, Eq. 6 is an optimal estimator. The standard deviations of the estimated parameters are determined according to Payne and Goodwin (1977),

$$\boldsymbol{\sigma}_{LS} = \sqrt{diag((\mathbf{X}^T\mathbf{X})^{-1}\sigma^2)}, \tag{7}$$

where σ^2 is a parameter of the distribution of the sum of the squares of the residuals S. A suitable unbiased estimator of σ^2 is proposed by Beck and Arnold (1977),

$$\hat{\sigma}^2 = \frac{(\mathbf{Y} - \mathbf{X}\hat{\boldsymbol{\theta}}_{LS})^T(\mathbf{Y} - \mathbf{X}\hat{\boldsymbol{\theta}}_{LS})}{n - p}, \tag{8}$$

where n is the number of discrete points and p, the quantity of parameters.

4. Experimental tests

The self-propelled tests were performed in a swimming pool of 10 m, 6 m and 1.80 m in length, width, and height, respectively. The tests were conducted in the 6-DOF of motion of the vehicle, 1-DOF at a time, to determine the drag force of the Hindrax ROV for different forces/torques applied by its propulsion system.

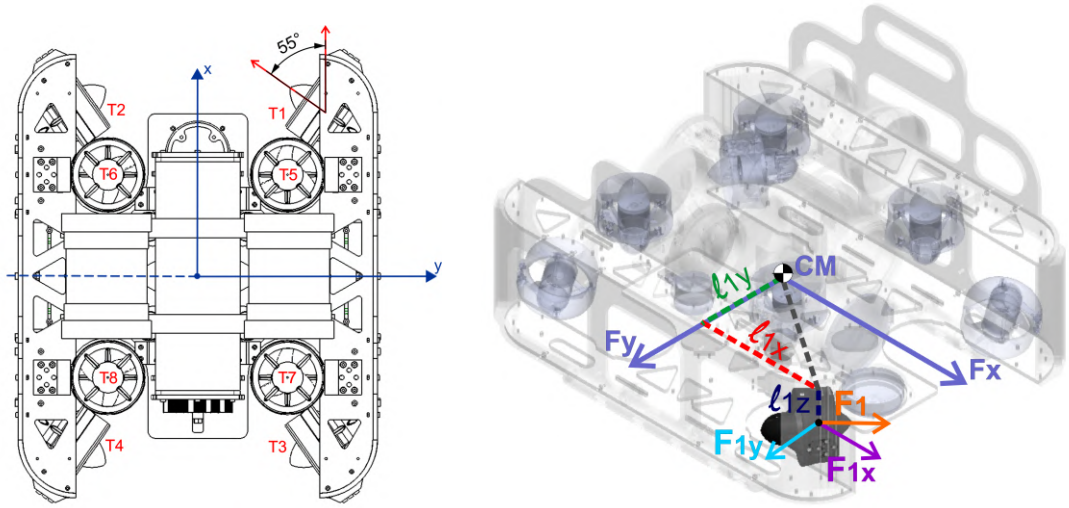

(a) (b)

Figure 5: (a) Configuration and numeration of thrusters. (b) Decomposition of the force in the thruster T1.

Figure 5a shows the thrusters configuration and numeration, and Figure 5b the decomposition of the force for the thruster T1. Let $F1$ be the thrust applied by T1 determined in Section 2.2.1, the vector $\mathbf{f} = [F_{1x}, F_{1y}, F_{1z}]^T$, the forces applied by T1 in the x, y and z axis and the vector $\mathbf{r} = [l_{1x}, l_{1y}, l_{1z}]^T$, the distances between the center of mass and the thruster T1 in the x, y and z axis. The forces and moments that is given by the thruster T1 in 6-DOF $\boldsymbol{\tau}_1$ can be determined by Fossen (1994) and Wu *et al.* (2018),

$$\boldsymbol{\tau}_1 = \begin{bmatrix} \mathbf{f} \\ \mathbf{r} \times \mathbf{f} \end{bmatrix} = \begin{bmatrix} F_{1x} \\ F_{1y} \\ F_{1z} \\ F_{1z}l_{1y} - F_{1y}l_{1z} \\ F_{1x}l_{1z} - F_{1z}l_{1x} \\ F_{1y}l_{1x} - F_{1x}l_{1y} \end{bmatrix} \tag{9}$$

The thrusters T1, T2, T3, and T4 have a rotation angle of 55°, as observed in Figure 5a. Therefore, the decomposition of the force of T1 is given by, $F_{1x} = cos(\alpha)F_1$, $F_{1y} = sen(\alpha)F_1$ and $F_z = 0$, where α is the rotation angle. The same procedure was used to calculate the force and moments applied by each thruster during the self-propelled tests.

4.1 Purely rectilinear motion

The self-propelled tests in the surge direction were performed by applying an input force through thrusters T1 and T2, while thrusters T4 and T5 controlled the heading. Figure 5a shows the configuration of thrusters. In sway, the input force was applied by thrusters T1 and T3, while thrusters T2 and T4 controlled the heading. The vertical thrusters T5, T6, T7, and T8 controlled the vehicle's altitude during the tests in the surge and sway directions; thus, the vehicle was submerged during those motions. The vehicle's distance to the pool bottom was between 1 and 0.8 m. The velocity of the vehicle in the surge and sway directions was measured with the DVL. The tests in the heave were conducted in the positive and negative directions (see Figure 2). The positive direction is when the vehicle goes down, and the negative when the vehicle goes up. The tests in the heave direction were performed using the vertical thrusters T5, T6, T7, and T8. In those tests, the vehicle's velocity was determined by deriving the altitude signal provided by the sonar.

4.2 Purely rotational motion

The angular velocity in the rotation tests was measured by the gyroscope and by deriving the angular position signals provided by the DVL. Those sensors are described in Table 1. The self-propelled tests in the yaw motion were performed by applying a torque to the vehicle through thrusters T1, T2, T3, and T4 (see Figure 5a with the thruster numeration) that

allowed the vehicle to rotate 360° around the z-axis clockwise. Figure 2 shows the frame of reference with the positive direction of the z-axis of the Hindrax ROV. As well as for the surge, sway, and heave self-propelled tests, the vertical thrusters T5, T6, T7, and T8 controlled the vehicle's altitude to be between 0.8 m to 1 m during the self-propelled test in the yaw motion.

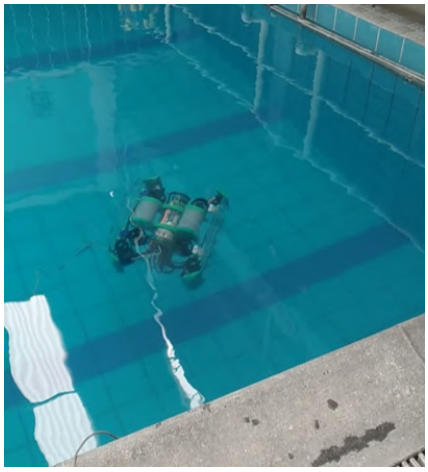

Figure 6: The Hindrax ROV during the self-oscillation test in the pitch motion.

The Hindrax ROV cannot make 360° rotation around the x and y axes (Figure 2 illustrates the frame of reference of the vehicle with the positive direction of the x and y axes). Therefore, the drag parameters in the roll and pitch motion were determined through self-propelled tests where the vehicle rotated up to 30° and 40°. In roll, the vertical thrusters T5, T6, T7, and T8, which configuration is in Figure 5a, applied a torque that led the vehicle to rotate around the x-axis clockwise up to 30°, and then the vehicle returned to its initial position. Similarly to roll, the same thrusters were used in pitch: T5, T6, T7, and T8. They applied a torque that led the vehicle to rotate around the y-axis clockwise up to 40°, and then the vehicle returned to its initial position. Figure 6 shows the vehicle during one of the self-propelled tests in pitch motion. The velocity signal measured during the rotations in roll and pitch showed that the signal became constant within the range of motion. In this way, Figure 7 shows the position and velocity signal obtained in one of the tests made in the roll motion. The velocity was constant in the angular position between -21° to -27°.

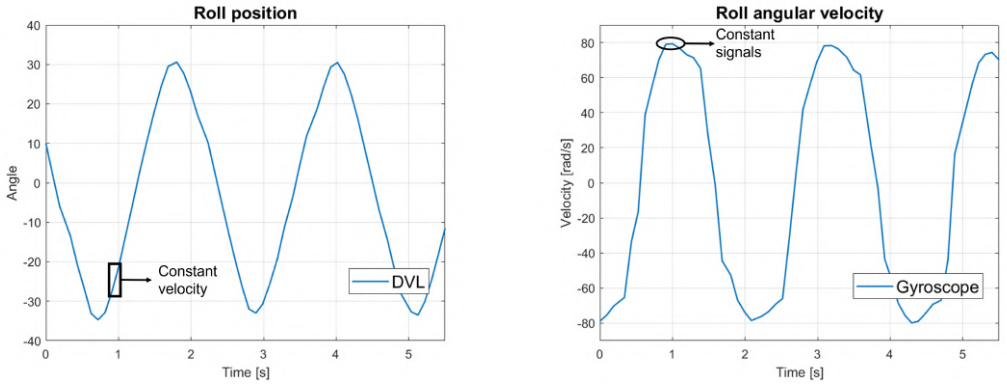

(a) (b)

Figure 7: Signal obtained of the self-oscillation test in roll of the (a) position and (b) angular velocity.

5. Results of the experimental tests

The curves of velocity vs force/torque to all DOF of the vehicle are shown in Figure 8, 9, 10. Figure 8a shows that the drag force is less in the surge direction than in the direction of sway in Figure 8b. However, the drag force in positive heave (see Figure 9a) is slightly higher than in sway. Such as to achieve 0.5 m/s, the positive heave and sway directions need around 25 N. The curves obtained in the direction previously mentioned are coherent with the projected areas of the vehicle because the minor projected area is in the surge direction that corresponds to the least drag force, and the projected area in positive heave and sway correspond similarly. This is observed in Figure 1 and 2.

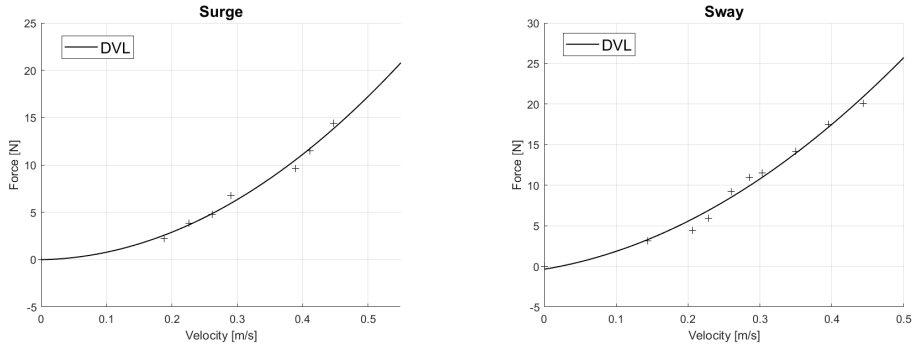

(a) (b)

Figure 8: Curves of force vs velocity: (a) surge; (b) sway.

Figure 9a and 9b show the drag force of the Hindrax ROV when it moved in the positive and negative direction of heave, respectively; The drag force is less in negative heave because this direction is not composed mainly of acrylic plates. It has an electronic pressure vessel, and the two floats with cylindrical shapes, see Figure 1a.

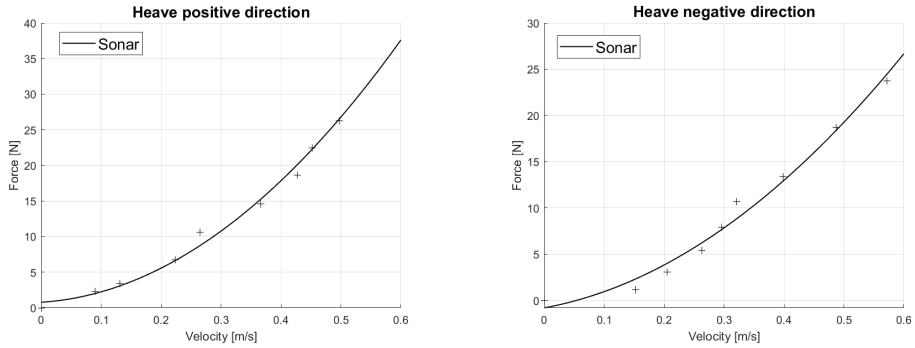

(a) (b)

Figure 9: Curves of force vs velocity: (a) positive heave; (b) negative heave.

The angular velocities of the roll, pitch, and yaw motion were measured by the gyroscope and by deriving the signal of position obtained by the DVL. Figure 10 compares the signals obtained from the DVL and the gyroscope, and there is no significant difference. The rotation tests in yaw were made in the clockwise direction; therefore, the area that came across those rotations corresponds to the lateral acrylic plate of the vehicle (see Figure 2). The drag force in this direction was higher than in roll and pith.

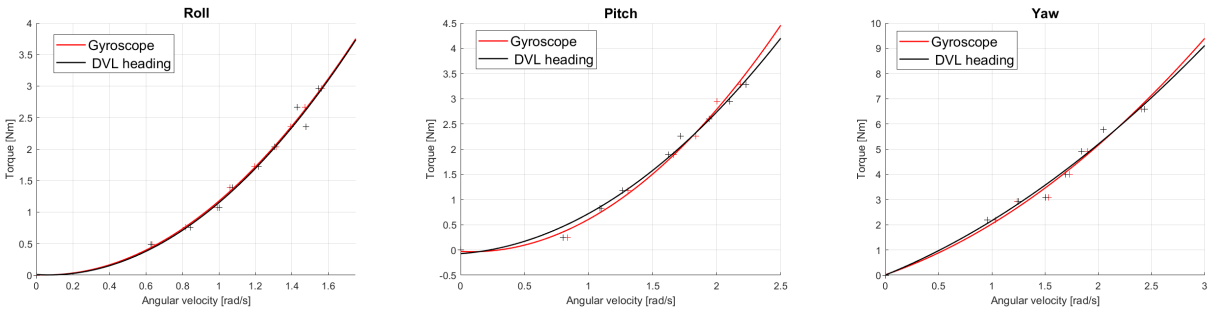

(a) (b) (c)

Figure 10: Curves torque vs angular velocity: (a) roll; (b) pitch; (c) yaw

The values of the linear and quadratic drag parameters of Eq. 2 are presented in Table 3. Those were determined by applying the LS method and the calculation of the standard deviations described in Section 4 from the data collected in all tests with constant velocity to each DOF.

The quadratic coefficient $k_{\xi|\xi|}$ is smaller in negative heave because the vehicle in this direction is composed of round

Table 3: Linear and quadratic drag parameter values estimated by the LS method of the Hindrax ROV.

Motion	$k_{\xi\|\xi\|}$	k_ξ	b_ξ
Surge (N)	66.48 ± 10.20	1.25 ± 4.97	-0.02 ± 0.58
Sway (N)	75.31 ± 14.54	14.54 ± 6.93	-0.36 ± 0.82
Positive heave (N)	93.52 ± 6.61	5.26 ± 4.71	0.77 ± 0.73
Negative heave (N)	56.57 ± 11.30	11.84 ± 6.97	-0.81 ± 0.99
Roll (Nm)	1.29 ± 0.06	-0.12 ± 0.11	0.006 ± 0.044
Pitch (Nm)	0.77 ± 0.08	-0.13 ± 0.19	-0.03 ± 0.10
Yaw (Nm)	0.55 ± 0.20	1.47 ± 0.50	0.02 ± 0.30

faces, being the pressure vessels and the floats (see Figure 1). The higher drag is in the positive heave direction because the projected area in this direction contains the acrylic plate of the vehicle with the largest area.

The standard deviations of the estimated parameter values show that sway and negative heave were higher than the standard deviations in the other directions. Experimental difficulties caused this; for example, when the vehicle moved in the sway direction, its motion was not always straight in velocities higher than 0.25 m/s, and as a result, the parameter b_ξ has its value as the second largest in Table 3. In the case of the negative heave, the main perturbation was due to the noise in the sensor because the velocity calculated by deriving the altitude signal presented oscillations. The calculated velocity in negative heave did not achieve a fully permanent regime because the depth of the pool was short; when the vehicle surfaced from the pool, the velocity was not in a fully permanent regime yet.

The higher value of the standard deviations of the quadratic drag parameters obtained in the rotation motions is for the yaw motion in Table 3. The noise in the magnetometer signal caused the perturbation due to the electromagnetic interference by the motors in the thrusters of the Hindrax ROV.

The values of b_ξ to the negative and positive heave motions correspond to the buoyancy force f_b of the Hindrax ROV because this force is not included in the mathematical model of Eq. 2 when the vehicle move in those directions. The parameter b_ξ model the difference between the weight of the vehicle W and the thrust of the vehicle as $f_b = W - \rho\forall$, where W is equal to 15.22 kg, $\forall$ is the volume of water displaced by the vehicle equal to 0.0153 m^3 and ρ, water density equal to 1000 kg/m^3. Thus, $f_b = 0.7845$ N. The relative error is 1% to 3%, comparing the referential value of the buoyancy force of the vehicle with the value b_ξ in the positive and negative heave in Table 3.

Table 4 shows the drag coefficients C_d and the Reynolds number Re of the tests. The second column corresponds to the mean and the standard deviations of the estimated drag coefficient to each DOF, and the third column is the Reynolds number range calculated during the self-propelled test.

Table 4: Mean values of the drag coefficients and the Reynolds number range of the self-propelled tests

Motion	C_D	Re range
Surge (N)	2.28 ± 0.21	$0.5 \times 10^5 - 1.1 \times 10^5$
Sway (N)	3.70 ± 0.33	$0.5 \times 10^5 - 1.1 \times 10^5$
Positive heave (N)	4.02 ± 0.74	$0.6 \times 10^5 - 1.8 \times 10^5$
Negative Heave (N)	2.48 ± 0.53	$0.4 \times 10^5 - 1.8 \times 10^5$
Roll (Nm)	0.039 ± 0.0015	$1.5 \times 10^5 - 4 \times 10^5$
Pitch (Nm)	$0.0224 \pm 6.7 \times 10^{-4}$	$2.5 \times 10^5 - 5.5 \times 10^5$
Yaw (Nm)	0.049 ± 0.011	$2.5 \times 10^5 - 6 \times 10^5$

The drag coefficient calculated to the linear motions was almost constant in the Reynolds number range between 0.4×10^5 to 1.8×10^5, and the drag coefficient calculated to the angular motion was almost constant in the Reynolds number range between 1.5×10^5 to 6×10^5.

6. Conclusions

This work applies an experimental method to identify the hydrodynamic drag parameters in the 6-DOF of the Hindrax ROV to the stock assessment of the Peruvian scallops and the mechanical and hardware description used to develop the tests with the vehicle. The experimental method used is known as self-propelled tests. Those tests consisted of applying different constant known forces/torques through the thrusters that let the vehicle make motions in the desired direction or rotation. The vehicle's on-board sensors measured linear and angular velocity during the tests. Then, the linear and quadratic drag parameters were determined using the LS method from the data collected in the self-propelled tests of each DOF. The drag coefficient calculated to the linear motions was almost constant in the Reynolds number range between

0.4×10^5 to 1.8×10^5, and the drag coefficient calculated to the angular motion was almost constant in the Reynolds number range between 1.5×10^5 to 6×10^5.

The drag parameter values found by the experiments are coherent because the higher parameter value corresponds to the larger projected area, and the lower parameter value to the smaller projected area. The experimental difficulties are reflected in the results found and were caused by the noise in the signals of the sensors, issues controlling the vehicle heading in the surge and sway directions, and the problem presented when the vehicle moved in the negative and positive direction of heave because the velocity signal did not achieve a fully permanent regime due to the reduced space. However, the parameter values b_ξ of positive and negative heave in Table 3, which is equal to the buoyancy force of the vehicle, presents a relative error of 3% with the buoyancy force, demonstrating that the procedure followed to determine the linear and quadratic parameters is valid, despite the experimental difficulties in heave.

The model proposed in Eq. 2 of the Hindrax ROV motion did not consider the loss force caused by the thruster-frame and thruster-thruster interactions and the on-board battery discharge. The vehicle has no sensor that lets us quantify the battery discharge; therefore, if the on-board battery started to discharge, the PWM signal sent to the thrusters would not generate the corresponding force. On the other hand, the distribution of the thrusters in the Hindrax ROV (see Figure 5a) allowed us to identify that the thruster-frame interaction is more significant for thrusters T5, T6, T7, and T8, and the thruster-thruster interactions, for T1, T2, T3, and T4. Those efficiency losses will be estimated in future works for being included in the mathematical model of the vehicle and a sensor will be installed in the vehicle to monitor the on-board battery level.

7. ACKNOWLEDGEMENTS

The authors would like to thank the CNPq for the scholarship financial support, the company VEOX, and their coworkers for the generous support and letting us the use of the installations and equipment to develop this work. It was performed within "Especial projects to the reactivation E067-2021-02, CONTRACT Nº 042-2021", financed by FONDECYT in Arequipa, Peru.

8. REFERENCES

Avila, J.P.J., Donha, D.C. and Adamowski, J.C., 2013. "Experimental model identification of open-frame underwater vehicles". *Ocean Engineering*, Vol. 60, pp. 81–94. ISSN 0029-8018.

Beck, J.V. and Arnold, K.J., 1977. *Parameter estimation in engineering and science*. JOHN WILEY & SONS.

Eng, Y., Lau, M., Low, E. and Seet, G., 2008. "Identification of the hydrodynamics coefficients of an underwater vehicle using free decay pendulum motion". *Lecture Notes in Engineering and Computer Science*, Vol. 2169.

Fossen, T.I., 1994. *Guidance and Control of Ocean Vehicles*. John Wiley & Sons.

Goheen, K.R. and Jefferys, E.R., 1990. "System Identification of Remotely Operated Vehicle Dynamics". *Journal of Offshore Mechanics and Arctic Engineering*, Vol. 112, No. 3, pp. 230–236. ISSN 0892-7219.

Miskovic, N., Vukić, Z., Bibuli, M., Bruzzone, G. and Caccia, M., 2011. "Fast in-field identification of unmanned marine vehicles". *Journal of Field Robotics*, Vol. 28, pp. 101 – 120.

Payne, R.L. and Goodwin, G.C., 1977. *Dynamic system identifications: Experiment Desgins and Data Analysis*. ACEDEMIC PRESS INC.

Randeni., S., Leong, Z., Ranmuthugala, D., Forrest, A. and Duffy, J., 2015. "Numerical investigation of the hydrodynamic interaction between two underwater bodies in relative motion". *Applied Ocean Research*, Vol. 51, pp. 14–24.

Ross, A., Hassani, V., Selvik, O., Ringen, E. and Fathi, D., 2015. "Identification of nonlinear manoeuvring models for marine vessels using planar motion mechanism tests". Vol. Volume 7: Ocean Engineering.

Wu, C.J., Eng, B. and Sammut, K., 2018. *6-DoF Modelling and Control of a Remotely Operated Vehicle*. Ph.D. thesis, College of Science and Engineering, Adelaide, Australia.

Zhandong, L., Jianguo, T., Hao, S., Yang, L. and Zongquan, D., 2017. "Hydrodynamic calculation and analysis of a complex-shaped underwater robot based on computational fluid dynamics and prototype test". *Advances in Mechanical Engineering*, Vol. 9, p. 168781401773450.

9. RESPONSIBILITY NOTICE

The authors are solely responsible for the printed material included in this paper.